Surface Winds at Landfall of Hurricane Andrew (1992)—A Reply

DA-LIN ZHANG

Department of Meteorology, University of Maryland, College Park, Maryland

YUBAO LIU AND M. K. YAU

Department of Atmospheric and Oceanic Sciences, McGill University, Montreal, Quebec, Canada

13 April 1998 and 10 July 1998

1. Introduction

We appreciate this opportunity to (i) clarify the simulation of surface winds at landfall of Hurricane Andrew (1992) as reported in Liu et al. (1997, hereafter referred to as LZY); (ii) make more detailed comparisons with one of the most sophisticated surface analyses of a landfallen hurricane by Powell and Houston (1996, hereafter referred to as PH96); and (iii) present the simulated winds at the surface and flight levels during the pre- and postlandfall periods. In LZY, we have shown that the model simulates the size of the eye reasonably well, the radius of maximum wind (RMW), and its asymmetry as well as the general distribution of surface winds with a peak magnitude greater than 65 m s^{-1} near the northern RMW–coastline intersection (see their Fig. 7), as verified against PH96's analysis. In addition, the model reproduces the rapid filling in central pressure and the rapid decrease in surface winds of the storm during Andrew's landfall (see Fig. 2 in LZY).

However, the model does not appear to produce *the surface wind discontinuity across the coastline* to the extent that was subjectively analyzed by PH96 (cf. Figs. 4b and 4c herein). It should be pointed out that the discontinuity in PH96, and other observational studies cited by Powell and Houston (1999, hereafter referred to as PH99), was *not obtained from direct observations.* We do not question the existence of pronounced changes in surface winds across the coastline, but we believe that their analyzed sharp discontinuity associated with intense normal-to-coastline flows and the absence of a transition zone downstream from the coastline are unrealistic and attributable to their ''converting the flight-level data using their boundary layer model over land and ocean, separately, and then merging them along the coastline without including full dynamics and physics interaction,'' as mentioned in LZY. In this reply, we will show that their converting the flight-level (at an altitude of 2.5–3.2 km) data with a simple, one-dimensional planetary boundary layer (PBL) model tended to introduce large errors in surface winds, while their merging, without considering a transition zone produced by horizontal momentum advection, accounts for the unrealistic sharp discontinuity. These problems could be clearly seen from their calculated vorticity and divergence fields. Yet, in their comments, PH99 choose not to address the above issues and our other concerns. Instead, they adopt the strategy of misinterpreting our simulated prelandfall winds and doubt (i) the Charnock constant used in MM5 to compute the surface roughness over ocean and (ii) our use of an 80-m thickness for the surface layer. They also comment on the mechanism by which the northern peak wind of >65 m s^{-1} is generated. Since LZY focus primarily on the general description and verification of the explicit simulation, little attention was paid to the landfall characteristics of Andrew. In this reply, we wish to explore in detail the changes in surface winds at landfall from our 72-h explicit simulation of Andrew, although a more detailed analysis of the landfall characteristics will appear in a separate journal article.

The next section describes briefly the treatment of the bottom boundary and surface friction in the PBL over land and ocean in order to better address PH99's concerns. In section 3, we show that PH99's estimation of the model parameters is inappropriate and invalid. We will also show that (i) our simulation reproduces the distribution of the often observed maximum surface winds prior to landfall very well; (ii) our model is capable of producing pronounced coastal discontinuity in surface isotachs but only under certain flow configurations, and (iii) there exists little relationship between the flight-level and surface winds. Differences between

Corresponding author address: Dr. Da-Lin Zhang, Department of Meteorology, University of Maryland, College Park, MD 20742-2425.
E-mail: dalin@atmos.umd.edu

TABLE 1. Description of land-use indices and surface parameters (adopted from Anthes et al. 1987) that are shown in Fig. 1.

Index	Description	Roughness (m)	Moisture avail. (%)	Albedo (%)	Emissivity (%)	Thermal inertia (cal m^{-2} K^{-1} $s^{-½}$)
2	Agriculture	0.15	30	17	92	400
3	Range/grassland	0.12	15	19	92	300
6	Mixed forest and wetland	0.40	35	14	95	500
8	Marsh or wetland	0.20	50	14	95	600

our simulation and PH96's analysis as well as limitations in their analysis will be also discussed. A summary and conclusions are given in the final section.

2. The PBL treatment and bottom boundary

The model we used is a nonhydrostatic, two-way interactive, movable, triply nested grid (i.e., 54/18/6 km) version of the Pennsylvania State University–National Center for Atmospheric Research (PSU–NCAR) Mesoscale Model (i.e., MM5; Dudhia 1993; Grell et al. 1995) with the finest grid size of 6 km and the Tao–Simpson (1993) cloud microphysics package. A modified version of the Blackadar (1979) PBL parameterization is incorporated (Zhang and Anthes 1982), in which the local tendency of the surface-layer-averaged momentum ($\mathbf{V}_a$) due to friction is represented by the vertical gradient of stress τ; that is,

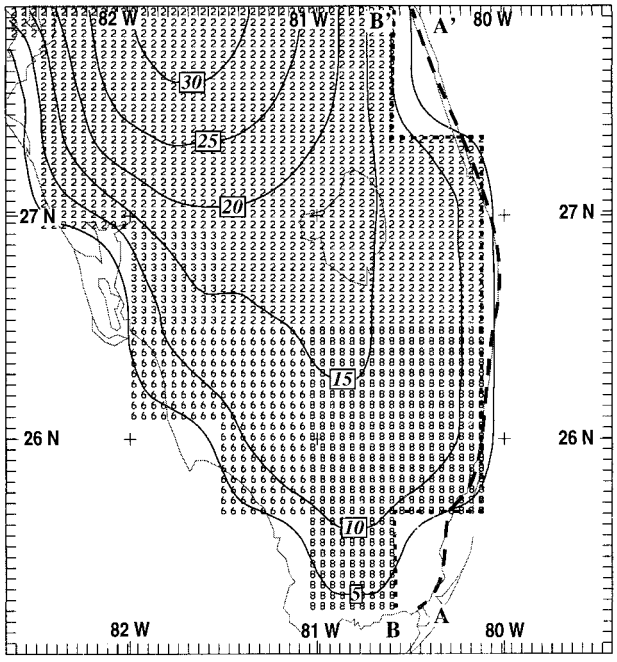

FIG. 1. Distribution of terrain (solid), at intervals of 5 m, and land-use indices (see Table 1 for pertinent description). Dashed line AA' represents the east coastline of Florida, whereas dotted line BB′ denotes the model coastline. The intervals between tick marks around the frame represent a grid length of 6 km. This interval is the same in all figures.

$$\left.\frac{\partial|\mathbf{V}_a|}{\partial t}\right|_{\text{Fric}} = \frac{1}{\rho}\frac{\partial\tau}{\partial z} = \frac{1}{\rho}\frac{\tau_1 - \tau_g}{z_1}, \tag{1}$$

where the subscripts 1 and g denote the top of the surface layer and the ground, respectively; and z_1 (=80 m in the present case) is the thickness of the surface layer. All prognostic variables are defined at half-σ levels (due to the use of a staggered grid configuration). The ground stress τ_g is calculated from

$$\tau_g = \rho u^{*2}, \tag{2}$$

where u^* is the friction velocity and computed in accordance with similarity theory; that is,

$$u^* = \frac{k|\mathbf{V}_a|}{\ln(z_a/z_0) - \psi_m}, \tag{3}$$

where k is the von Kármán constant, z_a (=40 m in the present case) is the (half-σ level) height of the surface layer, z_0 is the surface roughness length, and ψ_m is a stability parameter. We find from the model output that the magnitude of ψ_m, slightly negative (positive) over land (ocean) at landfall, is less than 5% of the logarithmic term in the denominator of Eq. (3). Thus, it is apparent from Eqs. (1)–(3) that u^* provides a measure of frictional effects, through surface roughness, on surface winds.

In MM5, the land surface temperature is predicted using a surface energy budget equation, in which surface fluxes of sensible heat, moisture, and momentum are computed from similarity theory [see Zhang and Anthes (1982) for more details]. The land surface roughness, together with other surface parameters (e.g., moisture availability, albedo, emissivity, and thermal inertia), is specified according to a land-use lookup table (see Table 1). It is evident from Fig. 1 and Table 1 that the eastern-half portion of Florida is categorized as marsh/wetland in the south and agricultural land in the north with the respective roughness lengths of 0.15 and 0.2 m. These values are generally comparable to the average values used by Powell et al. (1996) in their analysis of surface winds at Andrew's landfall.

Note that because of the use of two-way, movable nested grids, the bottom boundary conditions, together with all meteorological fields, in the leading portion of the 6-km grid-mesh domain have to be interpolated from its parent (18-km) grid-mesh domain every time (3 h in the present case) the fine grid moves during the model integration. Thus, the bottom boundary conditions

shown in Fig. 1 are equivalent to those in the 18-km grid-mesh domain and are obtained using NCAR's 10-min global terrain and land-use dataset. Apparently, this dataset shows the general distribution of terrain and land-use conditions over southern Florida reasonably well, but it does not accurately resolve the coastline of the Florida peninsula. In our simulation, the line BB', given in Fig. 1, represents the model's east coastline. Because of this inadequate resolution, we regrettably did not indicate in LZY the accurate location of the northern surface peak wind with respect to the coastline, as will be discussed in section 3. We believe that the relatively smooth terrain over southern Florida should have little impact on the distribution of surface winds in a hurricane during landfall.

Over ocean, the sea surface temperature (SST) is held constant in time during the integration. The surface sensible and latent heat fluxes are computed from the surface resistance law in a series configuration that consists of a near-surface molecular layer and the surface layer (see Carlson and Boland 1978), assuming a moisture availability of 100%. The surface friction velocity over the ocean is also calculated from Eq. (3) but using a roughness length in accordance with that given in Delsol et al. (1971); that is,

$$z_0 = au^{*2}/g + 10^{-4} \text{ m}, \quad (4)$$

where a is the Charnock constant ($a = 0.032$ herein). Some recent studies used $a = 0.0185$ (e.g., Bender et al. 1993), but we do not think that using this value would produce significant differences in surface winds offshore, because in nature, the oceanic z_0 can vary by two orders of magnitude from the center of the eye to the RMW of a hurricane.

Figure 2 shows the distribution of u^* at the landfall of Andrew obtained directly from the model output. The strong correlation between u^* and surface winds, as described by Eq. (3), can be clearly seen from the almost parallel alignment of the isotachs, given the relative uniform surface conditions over ocean or land. Of particular significance is the pronounced discontinuity in u^* across the coastline (due to the different roughness), especially over weaker flow (e.g., <50 m s^{-1}) regions, *except near the northern RMW–coastline intersection where a peak surface wind of >65 m s^{-1} offshore is present.* The friction velocity over the ocean varies from zero in the eye to 4.3 m s^{-1} just offshore in the northern peak wind region, as indicated by an arrow in Fig. 2. The corresponding roughness lengths are 10^{-4} m and 0.06 m, respectively. The latter magnitude amounts to 30% of the specified roughness length (i.e., 0.2 m) at the adjacent land points. It follows that differences in surface friction across the coastline should be much less evident at the RMW (or for intense flows) than elsewhere (or for weaker flows) inside the storm.

On the other hand, one may note the relative smoothness in surface isotachs across the coastline, particularly for winds greater than 40 m s^{-1}, which is in significant contrast to the pronounced discontinuity in u^* (Fig. 2). As will be seen in the next section, this relative smoothness in surface isotachs is caused by the dominant effect of horizontal momentum advection over that of surface friction. In fact, the relative significance of these two parameters in the momentum budget equation will be the key to understanding the limitations in PH96's analysis of surface winds across the coastline.

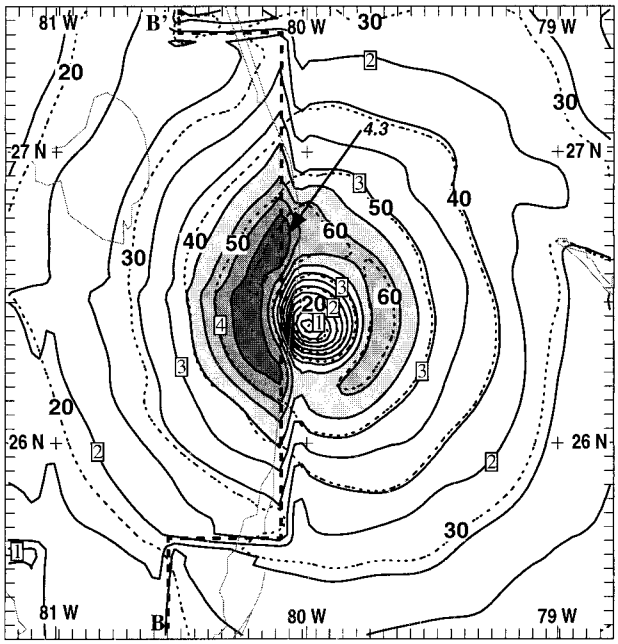

FIG. 2. Distribution of the surface friction velocity u^* (solid, every ⅓ m s^{-1}), superposed with surface wind speeds (dashed, every 10 m s^{-1}), obtained directly from the 68-h integration output, valid at 0800 UTC 24 Aug 1992 (i.e., at Andrew's landfall). Arrow indicates the magnitude of u^* associated with the northern peak surface wind of 65 m s^{-1}.

Given high vertical resolutions in the lowest troposphere, the Blackadar PBL scheme can explicitly simulate the vertical development of the boundary layer (with four different stability regimes). In the present case, six layers (centered at approximate half-σ level heights of 40, 121, 245, 454, 753, and 1243 m) are utilized to resolve the PBL structures in the lowest 1.5 km. Our detailed comparisons with available Omega dropwindsondes observations during Andrew's deepening show that MM5 with this resolution simulates the development of the maritime boundary layer in the vicinity of the storm (see Fig. 3 in LZY) reasonably well.

3. Surface winds during landfall

a. Use of a different surface framework for model verification

Since PH99 suggest that part of the differences in surface winds between our simulation and their analysis at landfall is caused by the use of a different framework

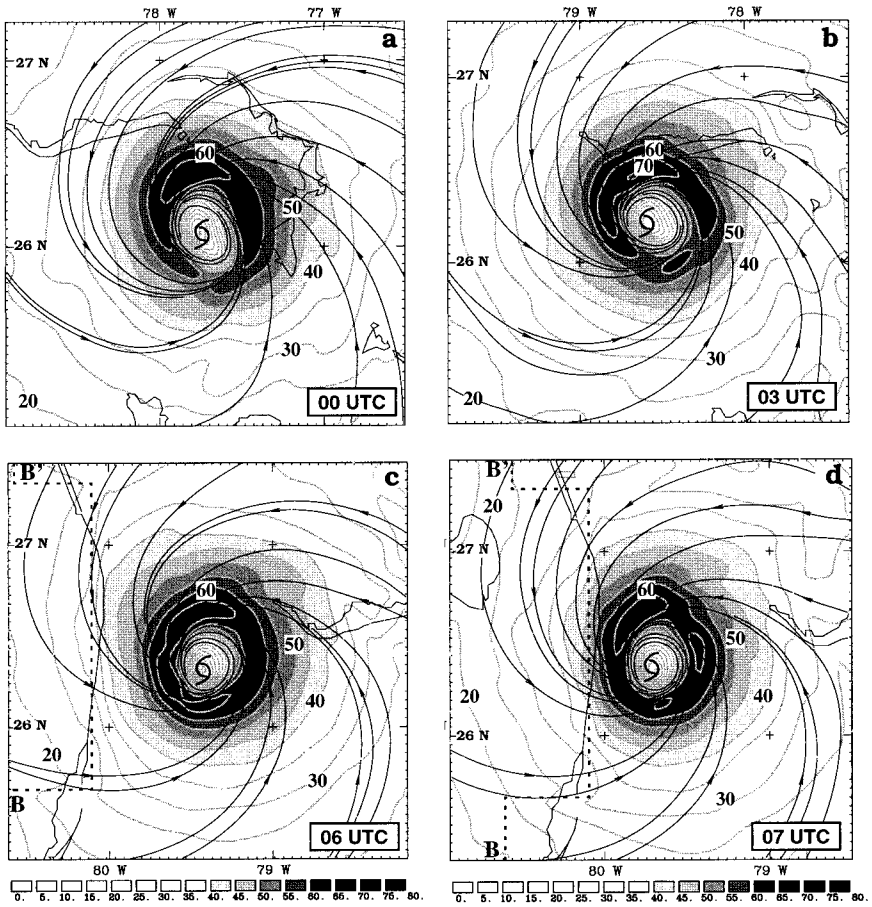

FIG. 3. Evolution of surface streamlines and isotachs (every 5 m s^{-1}) from (a) 60-h, (b) 63-h, and (c) 66-h, and (d) 67-h integrations, which are valid at 0000, 0300, 0600, and 0700 UTC 24 Aug 1992, respectively. Dotted line BB′ in (c) and (d) denotes the model coastline.

for model verification, it is necessary to discuss briefly the definition of surface winds in our simulation. Specifically, the surface winds in MM5 are defined at the lowest half-σ level ($\sigma = 0.995$ in the present case) at an altitude of 40 m following the terrain, and are representative of the winds averaged over a grid box (with a grid size of 6 km and a thickness of 80 m) and a time step (13.3 s). In addition, MM5 contains horizontal/vertical diffusion schemes and an Asselin-type time filter to reduce numerical aliasing for 2 to 4 $\Delta x/\Delta t$-scale noise. Thus, it is unnecessary to perform any further averaging for model verification; this is common sense to most numerical modelers.

On the other hand, observations taken at a particular point and instant generally contain high-frequency and small-scale noises. It is important to synthesize the observations, as was done by Powell et al. (1996) and PH96, through temporally averaging, time–space compositing, and vertical adjustment of the wind to an altitude of 10 m by assuming certain surface properties. However, PH96's final merging of land and ocean exposures by adjusting the flows at 10 m to a standard ''open terrain'' with a smaller roughness length resulted in surface winds equivalent to those at a higher level. Their results show that the surface winds increase systematically by >5 m s^{-1} after adjustment (see Figs. 3a–c therein), and our simulated surface winds are in better agreement with their adjusted winds.

It is also necessary to mention that the surface winds at the lowest σ level are not the exact winds at that height (i.e., 40 m), since they are obtained by treating the surface layer as an integral with similarity theory. Although numerical modelers customarily refer to the lowest model layer as the surface layer (e.g., Kurihara et al. 1990; Bender et al. 1993), such a definition is not rigorous. It may be desirable to use a 20-m thick surface layer centered at an altitude of 10 m, as suggested by PH99, but it is still debatable whether the layer-averaged surface winds at 10 m would be the same as the wind measured at a point at that height. Furthermore, we believe that the surface winds are much less sensitive to the thickness of the surface layer under the present hurricane environment of neutral and unstable conditions, as opposed to that under stable conditions, because in

the former cases the surface layer is coupled with the flows above in the PBL. Powell (1982) even found that his 10-m surface wind analysis of Hurricane Fredric (1979) compares favorably to the winds in the lowest model layer centered at an altitude of 500 m in the simulation of an idealized landfall hurricane by Moss and Jones (1978). Thus, it is inappropriate for PH99 to use the surface logarithmic law to interpolate our layer-averaged wind centered at 40 m to the wind at a point at 10 m. Their Table 1 obtained by using this interpolation is therefore invalid. To examine the effects of any model parameter, one has to perform sensitivity experiments with the three-dimensional model; in the present case, by varying the values of the Charnock constant and the surface layer thickness. We intend to report the results of such experiments in the future.

It should be mentioned that use of the 80-m surface-layer thickness represents a compromise between maintaining the validity of the constant flux assumption and reducing computational costs to satisfy the computational stability requirements. Similar and even larger surface thicknesses have also been used in previous numerical hurricane studies (e.g., Tuleya et al. 1984; Bender et al. 1985).

b. Evolution of surface winds prior to landfall

PH99 indicate that for a storm, like Andrew, moving at a speed greater than 5 m s^{-1}, the maximum surface winds should be maintained in the north semicircle or northwestern quadrant. Here, we are pleased to report that even with the National Centers for Environmental Prediction (previously known as the National Meteorological Center) analysis as the model initial conditions, MM5 reproduces the often observed maximum surface winds in the northwest quadrant prior to landfall very well, as shown in Figs. 3a,b. For example, our 60- to 63-h simulations show that the peak surface winds of about 70 m s^{-1} are located at the RMW in the northwestern quadrant (Figs. 3a,b). An examination of our hourly model output during a 36-h period prior to landfall reveals that more intense surface winds always occur in the north semicircle but with the peak winds appeared most often in the northwestern quadrant and sometimes oscillated into the northeast quadrant (not shown). Only at 0600 UTC 24 (Fig. 3c), intense surface winds of greater than 65 m s^{-1} have spread *temporally* into the west semicircle of the storm; but the local maximum is still situated in the northwestern quadrant. In fact, shortly after this hour but prior to landfall (i.e., at 0700 UTC 24), the maximum surface winds are clearly evident in the northwestern quadrant (Fig. 3d), which are the exact type of structures as PH99 indicated.

However, PH99 ignore the model-produced *persistent* surface wind structures, for example, as those shown in Figs. 3a,b and 3d; instead, they focus on the *transient* wind structure in the west semicircle that occurs only at 0600 UTC, as given in Fig. 3c, and use it to mislead the reader that our model produces ''a distinct prelandfall wind distribution that differs both from the observations and earlier hours of the simulation.'' This appears to be PH99's important strategy in defending their analyzed sharp discontinuity by criticizing our simulated prelandfall surface winds, but without providing any observation near 0600 UTC. Thus, we will leave it to the reader to judge the quality of our simulated surface winds and the credibility of PH99's criticism. We should mention, though, that the peak surface winds do begin to shift into the west semicircle, but after landfall (cf. Figs. 3d and 4b). Nevertheless, the more intense winds above 1–2 km are still persistently located in the north semicircle during the final 36-h integration period (e.g., see Figs. 6 and 7).

c. Surface winds at landfall

Now, let us examine the simulated surface wind structures and evolution at and after landfall, as compared to the PH96 analysis. Figure 4a displays the distribution of surface winds at landfall, which is the same as Fig. 7b in LZY except for the different domain sizes and the added model coastline. For the convenience of comparison, PH96's surface analysis is given in Fig. 4c. (Note the different domains used between the simulation and the analysis due to our simulated landfall position error of about 100 km.) Of importance is that the more intense surface winds at the RMW in the northwestern quadrant have reduced in intensity and area coverage as the storm moves over land (cf. Figs. 3d and 4a), clearly reflecting the impact of frictional dissipation. Figure 5b shows that surface friction appears to have induced large cross-isobaric flows, especially in the eyewall. Of further importance is that a small region with wind speed greater than 65 m s^{-1} is still present near the northern coastline–RMW but in a location offshore. We acknowledge that this peak-wind region was mistaken in LZY as land points because we did not use the land-use data to determine the model coastline; *this peak wind is located just between the real and model coastlines* (Fig. 4a). On this issue, we appreciate PH99's expert comment, since this one-grid-length difference reveals quite different stories about the influence of surface friction on the surface winds. Although this peak wind region should be regarded as the remnant of the earlier robust eyewall circulation, it does coincide with an inland maximum surface convergence (see Fig. 5a) or an inland updraft center in the eyewall (two grid lengths) downstream (see Fig. 6, to the left of point B'), as mentioned in LZY. Therefore, with this clarification, we may state that the region of simulated peak surface flow at landfall, occurring offshore, is realistic and in excellent agreement with PH96's analysis (cf. Figs. 4a and 4c). Evidently, the excellent predictability of this localized peak wind region offshore is obtained not by chance, since it results from the interaction of persistent intense surface flows with the land–ocean contrast. This

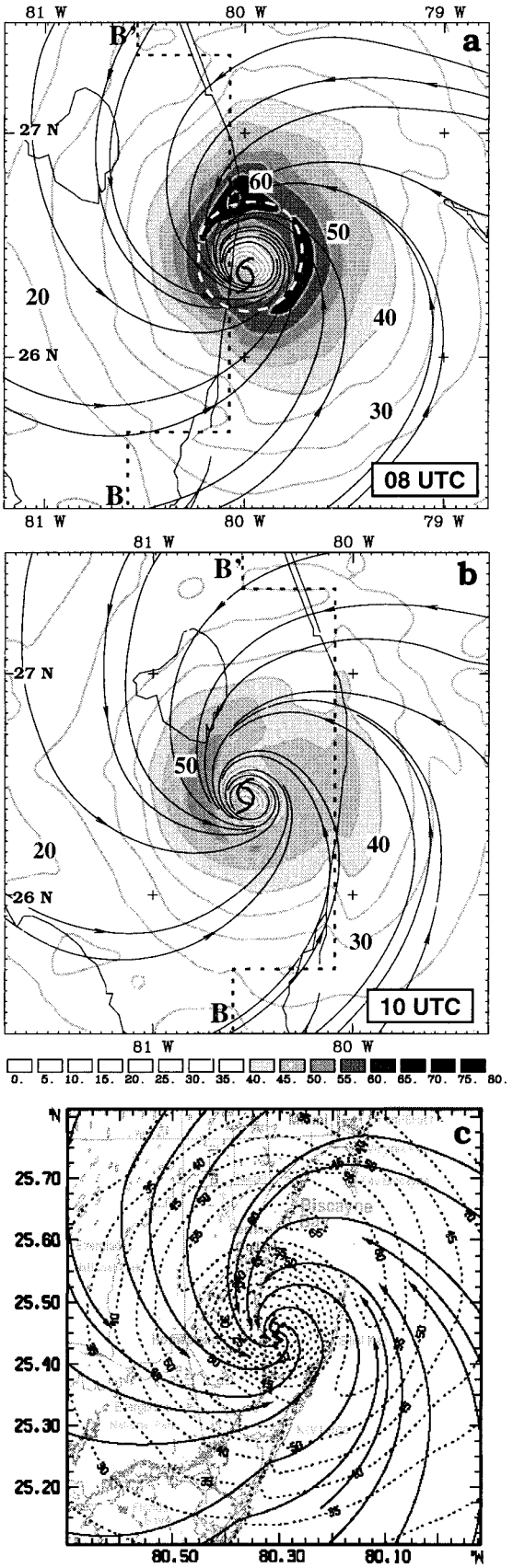

phenomenon must be reproduced by use of realistic processes in the model, such as cloud microphysics and PBL, given the observed SST and other large-scale conditions.

MM5 also realistically produces the often observed coastline asymmetries at landfall, as can be seen from the shape of the isotachs at landfall (Fig. 4a). In addition, the RMW in the southwest quadrant shrinks significantly, with much greater wind gradients occurring over land than over ocean. Of more relevance is the coastline asymmetry in wind speed at the RMW. Specifically, the model produces an elongated zone of intense flow (i.e., >60 m s^{-1}) that penetrates into the land at the northern coastline–RMW where the flow is directed from ocean to land, whereas to the south the inland weaker flow region is well extended into the ocean, as the winds blow from land to ocean, such that the surface flow at the RMW offshore weakens by about 10 m s^{-1} during the previous 1 h (cf. Figs. 3d and 4a). This phenomenon (i.e., a transition zone downstream from the coastline) must be caused by horizontal advection of momentum, though strongly influenced by the underlying surface roughness. (The pressure gradient force associated with the land–ocean contrast should be small.) However, this advective effect was not included in PH96's *horizontal merging* near the coastline. Instead, their analysis assumes immediate adjustment of the surface flow to the underlying surface forcing, (i.e., land and ocean exposures), so sharp discontinuity was placed across the coastline even *with a portion of the surface isotachs coinciding with the coastline.* This appears at the RMW both near the northern peak wind region and immediately offshore in the south.

In the present case, should we expect the model to produce such sharp discontinuity at the RMW–coastline near the landfall of Andrew's eye (even with the Charnock constant $a = 0.0185$ and the surface-layer thickness suggested by PH99)? Our answer is no. First, as discussed in section 2, the intense flow at the RMW tends to produce small differences in surface roughness and frictional velocity across the coastline (Fig. 2). With wind speeds of 65 m s^{-1} offshore and 60 m s^{-1} at the adjacent land point (see Fig. 4a), the difference in u^* should be less than 0.3 m s^{-1} near the northern RMW–coastline intersection, which is at most similar to the u^* gradient over land (see Fig. 2). Second, from the consideration of advection, the cyclonic circulation at this stage is relatively symmetric with respect to the coastline. Hence, air parcels in the surface layer enter or exit the land with large angles across the coastline. It will

←

FIG. 4. As in Fig. 3 but for (a) 68-h and (b) 70-h integrations, which are valid at 0800 and 1000 UTC 24 Aug 1992, respectively. (c) The composited surface analysis at 0900 UTC 24 Aug 1992 (adapted from PH96). Dashed lines in (a) denote the distribution of the RMW.

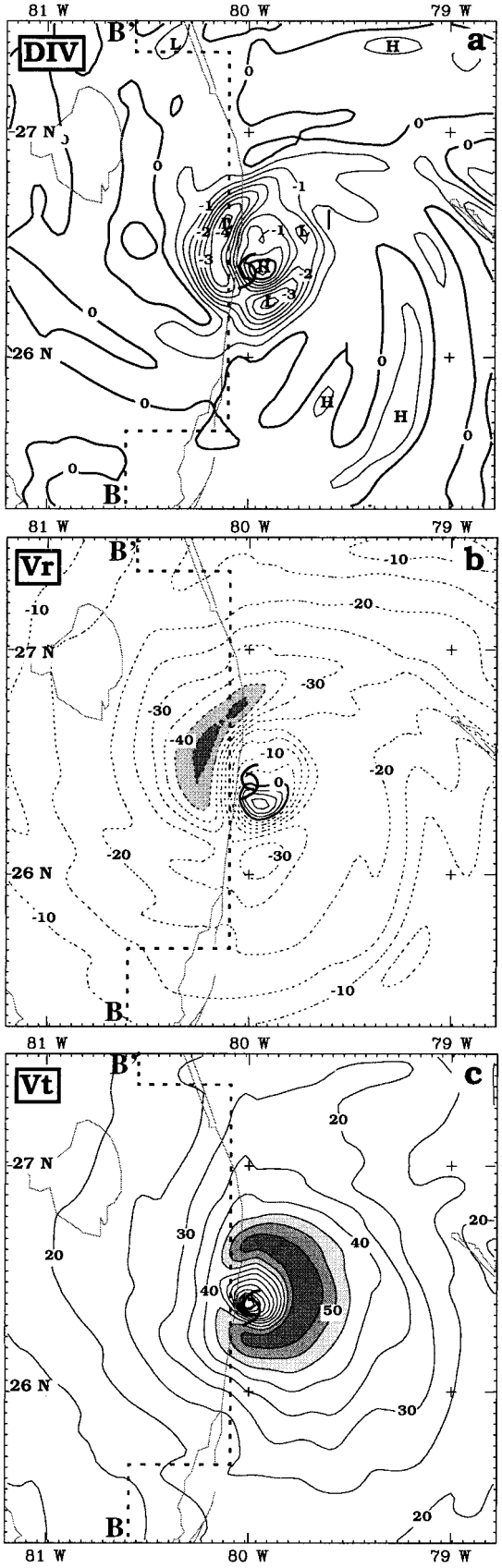

take some time for them to adjust completely to the underlying surface conditions, during which time air parcels would have been advected over a certain distance, resulting in the formation of a transition zone (about 12–18 km in the present case, as estimated by extending the isotachs at the RMW in the south onshore under the axisymmetric assumption). (Note that the transition zone could be much narrower if a smaller grid size is used.) In other words, the advective processes in the presence of intense flow could overcompensate for the frictional processes described by Eq. (1) in determining the surface winds in the transition zone downstream from the coastline. Of course, this advective effect is small in weak circulations compared to the frictional forcing induced by more abrupt changes in surface roughness across the coastline. For a similar reason, one may expect a larger discontinuity in surface isotachs when surface winds have a small component normal to the coastline. It follows that a *large discontinuity in surface isotachs tends to occur when either (i) the surface winds are moderate; or (ii) the surface winds across the coastline have a significant period (or distance) of different land or ocean exposures.*

To substantiate the above arguments, we present in Fig. 4b the streamlines and isotachs of the surface flow nearly 2 h after landfall. It is apparent that the model is capable of producing a *large discontinuity* in surface winds associated with the differential surface friction across the coastline, but with a transition zone of 12–18 km offshore. This is in marked contrast to the PH96-analyzed discontinuity in surface isotachs coinciding with the coastline (cf. Figs. 4a–c). Note that the discontinuity is greater in the south, where the surface flows at both sides of the coastline are going through a significant period (or distance) of different PBL processes, than in the north where the horizontal advective effect, though weak, is not negligible (Fig. 4b). Such discontinuity also appears, to a certain degree, at earlier hours some distance away outward from the RMW (see Figs. 3c,d and 4a). In general, the weaker the surface flow or the more the surface winds are aligned parallel to the coastline, the greater is the discontinuity. This result is consistent with previous idealized modeling studies of tropical cyclones at landfall, (e.g., Tuleya and Kurihara 1978; Tuleya et al. 1984; Bender et al. 1985). A comparison between Figs. 4a,b indicates that the surface winds have weakened substantially during the 2-h period after landfall; *the maximum surface wind decreases by approximately 25%* (i.e., from about 65 to 50 m s^{-1}). The inland peak wind of 50 m s^{-1} in Fig.

←

FIG. 5. As in Fig. 2 but for (a) the divergence (every 0.5×10^{-3} s^{-1}; convergence shaded); (b) radial component (every 5 m s^{-1}; inflow >40 m s^{-1} shaded); and (c) tangential component (every 5 m s^{-1}; >45 m s^{-1} shaded) of the surface flow. Dotted line BB′ denotes the model coastline.

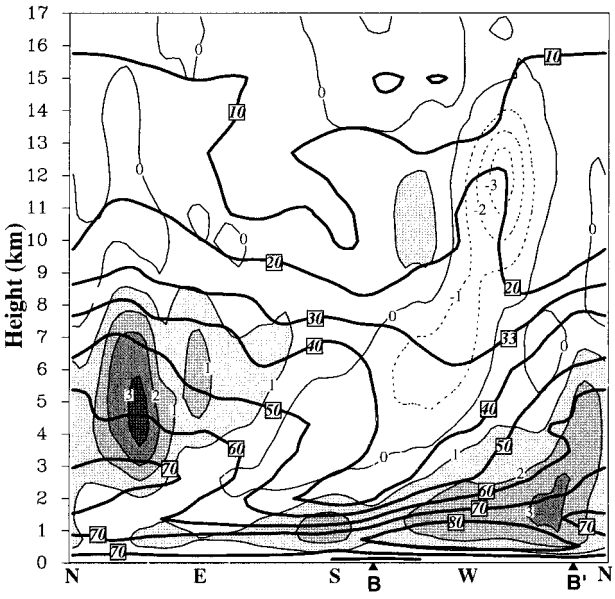

FIG. 6. As in Fig. 2 but for the azimuth–height cross section of horizontal wind speeds (thick solid) and vertical motion (thin solid; upward motion shaded) that is taken at the RMW as indicated in Fig. 4a. Letters B and B' denote the intersection of the RMW with the model coastline to the south and north of the storm, respectively.

4b conforms to the observed maximum surface winds over southern-central Florida (see Fig. 6 in PH96).

To further verify whether our model produces the right surface flow structures along the coastline, it is desirable to examine the distribution of divergence at Andrew's landfall, since a large discontinuity implies the presence of intense convergence. One can see from Fig. 5a that the modeled Andrew is characterized by an extensive area of convergence within a radius of 50 km from the center, except in the eye where weak divergence dominates. The most intense convergence occurs over land in the eyewall. Its center is located two grid lengths downstream from the northern peak wind region (cf. Figs. 5a and 4a). It is important to note that the distribution of convergence shows little relationship to the orientation of the coastline, indicating that the eyewall dynamics dominate over the convergence generated by the land–water contrast. This inland intense convergence is consistent with the model-generated large friction velocity in the eyewall (cf. Figs. 2 and 5a), so it is attributable to strong cross-isobaric flows induced by surface friction that are well represented by the storm's radial inflows (cf. Figs. 5a,b). Note that the maximum convergence of about 4×10^{-3} s^{-1} appears inward from the center of the radial inflow, that is, where radial gradient of the inflow is large. This reveals that the surface convergence is more related to the radial than tangential component, except near the coastline (cf. Figs. 5a–c).

In contrast, PH96's analysis shows a region of widespread, elongated surface convergence centered along the coastline, which is consistent with their analyzed sharp wind discontinuity (see their Figs. 3c and 4a). A similar elongated convergence structure, but maximized in Andrew's eye, was also analyzed along the coastline upon the exit of Andrew from southwest Florida (see their Fig. 5). Both of these results illustrate PH96's implicit assumption of the importance of the interaction of a hurricane vortex with the land–ocean contrast (i.e., associated with surface friction), rather than eyewall dynamics. Unfortunately, their analysis does not appear to be consistent with the observations. Specifically, the strongest convergence, having a value greater than 5×10^{-3} s^{-1}, was analyzed at the coastline immediately downstream from the northern offshore peak wind region. Since this value is equivalent to an upward motion of 0.5 m s^{-1} at an altitude of 10 m, it is inconceivable that *there is little indication of intense deep convection over this region.* The same can be said about their analyzed large convergence in the eye upon the storm's exit. Furthermore, even from the consideration of pure frictional effects, our model-generated gradient in u^* near the northern peak wind region, given in Fig. 2, does not support the existence of such intense convergence at the coastline.

We also noted that their analysis differs from our simulation by exhibiting much weaker convergence (about 10^{-3} s^{-1}) in the eyewall and no evidence of divergence in the eye, probably on account of the lack of high-resolution surface observations. This limited resolution problem is further illustrated in their analyzed maximum vorticity at the center of the hurricane vortex (see their Fig. 4b), as opposed to its occurrence in the eyewall in the numerical simulation (see Fig. 15d in LZY). From the consideration of the results of our high-resolution, dynamically consistent simulation dataset and the argument presented above, it becomes evident that there exists limitations in compositing the different types of observations for surface wind analysis. In other words, the composite observational data of PH96 could provide a reasonable description of the storm-scale surface flow structures, but could not properly resolve certain mesoscale features, such as the intense convergence and cyclonic vorticity in the eyewall, the weak divergence in the eye, a transition zone downstream from the coastline, wind intensity changes, and the convergence pattern across the coastline. Unfortunately, PH99 choose not to address the above problems related to their analyzed sharp discontinuity in surface winds. It should be pointed out, though, that some of the above inconsistencies might be caused by the fact that small errors in the wind analysis could produce large differences in divergence or other high-order moment variables; so care must be taken to compute them using raw observations.

To provide a more complete understanding of the changes of surface winds at landfall, we present in Fig. 5c the distribution of the storm's tangential flow. It is evident that while the radial inflow increases over land at Andrew's landfall, the weakening of surface winds

due to the frictional effect occurs mainly in the tangential component (cf. Figs. 4a and 5c). Differences in tangential winds at the RMW across the eye between land and ocean are greater than 20 m s^{-1}, whereas their differences in total speed are about 5 m s^{-1}. It should be mentioned that our result does not support the hypothesis of Wakimoto and Black (1994) that the increased surface friction may lead to a transient intensification of the surface tangential winds after landfall. Again, pronounced asymmetries in both the tangential and radial flows are apparent across the coastline.

d. Any relationship between the flight-level and surface winds?

Finally, we wish to show that some of the limitations in PH96's analysis could be partly attributed to the use of flight-level observations to infer the surface winds through a simple PBL model. It should first be pointed out that (i) an altitude of 2.5–3.2 km (i.e., the flight level) in hurricanes could hardly be considered as part of the PBL; and (ii) it is not even possible to infer the surface wind from that at an altitude of 1–2 km under clear-sky conditions without knowledge of the geostrophic forcing, let alone relate the surface and flight-level winds under highly convective situations. Nevertheless, an azimuth–height cross section of total wind speeds and vertical motion at landfall is given in Fig. 6, which shows the highly asymmetric flow structures at the RMW and the nonuniform distribution of winds with height. The cyclonic flow peaks at an altitude of 800 m with a magnitude greater than 80 m s^{-1} over land (i.e., near point W). It then decreases to a value of 45 m s^{-1} at an altitude of 3 km, a magnitude *nearly half* of that at the jet level. Despite the vertical slantwise-wind structures, Figs. 6 and 7 show that intense flows between 500 m and 6 km are systematically located in the north semicircle, as often observed (see PH99), though with different azimuthal extent in the vertical. In particular, the flight-level azimuthal wind distribution differs substantially from that at the surface (cf. Figs. 4a, 6, and 7). Thus, there exists little quantitative relationship between the flight-level and the surface winds. Franklin et al. (1999) also reach the same conclusion, based on their analyses of multiple Global Positioning System (GPS) dropwindsondes in the eyewall of hurricanes. These results suggest that *to reasonably incorporate flight-level observations into the surface analysis, aircraft have to fly near the jet level* (i.e., 800–1200 m). Figure 6 also shows the significant impact of horizontal advection; namely, isotachs and the vertical motion field tend to tilt downshear, particularly in the lower troposphere, in spite of the concentrated intense flow in the north semicircle. For example, a penetrative downdraft initiates at an altitude of 16 km in the northwest quadrant and then descends cyclonically to a height of 2 km in the east. The downshear-tilt characteristics make it more difficult to reasonably infer the surface wind information from the flight-level data. Liu et al. (1999) provide a more detailed discussion on the asymmetric flow structures at different radii during the storm's intensifying stage.

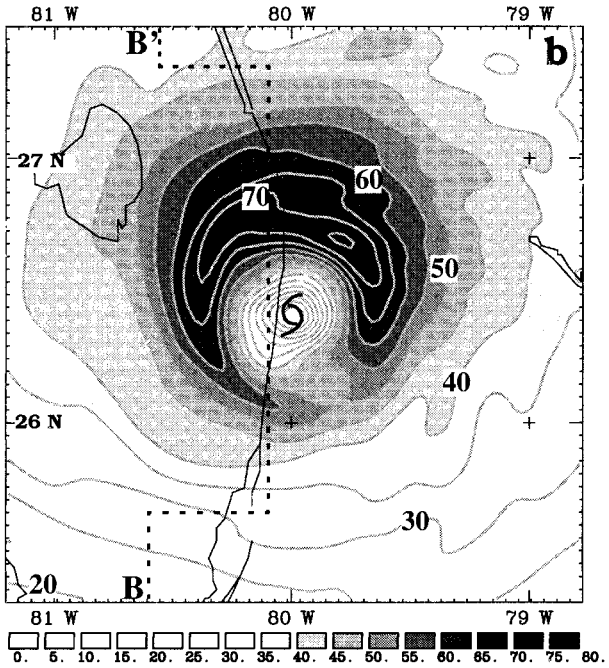

FIG. 7. As in Fig. 2 but for horizontal wind speeds at an elevation of 3.4 km.

It is also evident from Figs. 6 and 5a that a relatively strong/deep updraft (>3 m s^{-1} at 1.5 km), corresponding to the maximum surface convergence, is located over land to the north (i.e., to the left of point B'), as mentioned previously. On the other hand, a weaker/shallow updraft center associated with weaker convergence is located to the south at the coastline (i.e., at point B). (Note that Fig. 6 could not show the distribution of midlevel intense updrafts because of the sloping nature of the simulated eyewall; see Fig. 10 in LZY.) The different characteristics in vertical motion appear to be caused partly by the contrasting frictional effects and flow directions across the coastline at the two locations (see Figs. 2, 4a, and 6). Of course, the intense inland updraft must have been significantly enhanced by latent heat release in the eyewall.

4. Summary and conclusions

In this reply, we have presented the structures and evolution of simulated surface winds prior to and during landfall of Hurricane Andrew (1992) and compared them to PH96's analysis and other observations. It is shown that MM5 reproduces well the general distribution of surface winds and the often observed coastal asymmetries at landfall, including the noncircular shape of the isotachs, the onshore decrease of the RMW, dif-

ferent wind speeds between the northern and southern coastline–RMW, and different radial and tangential components as well as the convergence pattern across the coastline. Unlike what PH99 speculated, MM5 also reproduces the often observed maximum surface winds in the north semicircle or northwestern quadrant prior to landfall.

It is also shown that the model is capable of simulating a large discontinuity in surface winds across the coastline due to the differential surface friction but with a transition zone downstream from the coastline or offshore. In particular, we have demonstrated the importance of horizontal advection of momentum in ''smoothing'' out the wind discontinuity (or generating the transition zone) downstream from the coastline at landfall, when the cyclonic circulation is relatively symmetric with respect to the coastline. We argued that a large discontinuity in surface winds tends to occur along the coastline when either (i) the surface flows are moderate, or (ii) the coastal surface flows are directed more parallel to the coastline. However, one should not expect such discontinuity in the presence of intense normal-to-coastline surface flows because of the weak gradients in surface friction across the coastline and the significant advective effects. Our results suggest that a transition zone with different curvatures that are compatible with the magnitudes of surface winds should be analyzed downstream from the coastline or offshore.

Our simulation reveals that the surface-friction-induced convergence (and radial inflow) is maximized in the eyewall, rather than along the coastline. The simulation exhibits significant weakening of surface winds after landfall. We acknowledged that because of using the 10-min resolution land-use data that fail to accurately resolve Florida's coastline, the strongest wind in the northern eyewall, mentioned in LZY as being located over land, should be described as occurring just offshore. With this clarification, the simulated localized peak surface winds offshore are found to be in excellent agreement with PH96's analysis. This result indicates that the excellent predictability of this phenomenon is obtained not by chance (but by use of realistic processes in the model, such as cloud microphysics and PBL), since it results from the interaction of persistent intense surface flows with the land–ocean contrast. In conclusion, we may state that (a) our model reproduces the surface winds prior to and during Andrew's landfall reasonably well, including the wind structures across the coastline; and (b) PH99's concerns mentioned in the introduction, based on their misinterpretation of our model parameters and simulation results, are invalid.

Furthermore, detailed comparisons of our simulation with PH96's surface analysis reveal several problems and limitations with their dataset, which was composited from different sources under various assumptions. In particular, their analysis appears to overemphasize the importance of the interaction of a vortex with the land–ocean contrast, as compared to the eyewall dynamics. Their analyzed sharp discontinuity in surface winds (with a portion of the surface isotachs coinciding with the coastline) is shown to result from their merging of land and ocean exposures without considering the roles of horizontal momentum advection in generating a transition zone downstream from the coastline. The intense convergence/divergence so obtained along the coastline is not consistent with both the observed convective distribution and the eyewall dynamics. Although PH96's analysis provides an excellent description of the storm-scale cyclonic circulations, it fails to resolve wind intensity changes across the coastline, the intense convergence and cyclonic vorticity in the eyewall, as well as the weak divergence in the eye, due partly to the limited resolution in surface observations and partly to their overemphasis on the importance of the land–ocean contrast. Our simulation reveals little quantitative relationship between the flight-level and surface winds. To reasonably incorporate flight-level observations into the surface analysis, aircraft have to fly near the peak wind level (i.e., 800–1200 m). Otherwise, such data should be incorporated into a dynamical hurricane model through four-dimensional data assimilation, rather than by a simple, one-dimensional, PBL model. These comparative analyses suggest that it may be desirable for observational analysts to use four-dimensional, high-resolution model data, like ours, to guide their analysis of certain unresolved meteorological features in tropical storms and develop their associated conceptual models.

It should be mentioned that although the model simulates the air–land and air–sea interactions reasonably well, several areas of improvement could be made to produce a more realistic simulation of the landfall characteristics of Hurricane Andrew (1992). These include an increase in model resolution, the use of higher-resolution terrain and land-use data, the coupling of atmospheric and oceanic models, the incorporation of dissipative heating and sea spray evaporation, and a more accurate simulation of the landfall location of the storm. It should also be mentioned that because of these limitations, we do not claim that MM5 exactly reproduces the surface winds across the coastline. A verification and better understanding of the surface winds at landfall of hurricanes may have to wait until high-resolution (preferably at 1–2 km) surface observations become available.

Acknowledgments. This work was supported by the Natural Science and Engineering Research Council of Canada NSF Grant ATM-9802391, and the U.S. Office of Naval Research. The computations were performed at the National Center for Atmospheric Research, which is sponsored by the National Science Foundation.

REFERENCES

Anthes, R. A., E.-Y. Hsie, and Y.-H. Kuo, 1987: Description of the Penn State/NCAR Mesoscale Model version 4 (MM4). NCAR Tech. Note NCAR/TN-282, 66 pp.

Bender, M. A., R. E. Tuleya, and Y. Kurihara, 1985: A numerical study of the effect of a mountain range on a landfalling tropical cyclone. *Mon. Wea. Rev.,* **113,** 565–582.

——, R. J. Ross, R. E. Tuleya, and Y. Kurihara, 1993: Improvements in tropical cyclone track and intensity forecasts using the GFDL initialization system. *Mon. Wea. Rev.,* **121,** 2046–2061.

Blackadar, A. K., 1979: High resolution models of the planetary boundary layer. *Advances in Environmental Science & Engineering,* Vol. 1, Gordon and Briech Science Publications, 50–85.

Carlson, T. N., and F. E. Boland, 1978: Analysis of urban-rural canopy using a surface heat flux/temperature model. *J. Appl. Meteor.,* **17,** 998–1013.

Delsol, F., K. Miyakoda, and R. H. Clarke, 1971: Parameterized processes in the surface boundary layer of an atmospheric circulation model. *Quart. J. Roy. Meteor. Soc.,* **97,** 181–208.

Dudhia, J., 1993: A nonhydrostatic version of the Penn State–NCAR Mesoscale Model: Validation tests and simulation of an Atlantic cyclone and cold front. *Mon. Wea. Rev.,* **121,** 1493–1513.

Franklin, J. L., M. L. Black, and S. E. Feuer, 1999: Wind profiles in hurricanes determined by GPS dropwindsondes. Preprints, *23d Conf. on Hurricanes and Tropcial Meteorology,* Dallas, TX, Amer Meteor. Soc., 167–168.

Grell, G. A., J. Dudhia, and D. R. Stauffer, 1995: A description of the fifth generation Penn State/NCAR Mesoscale Model (MM5). NCAR Tech Note-398 + STR, 138 pp.

Kurihara, Y., M. A. Bender, R. E. Tuleya, and R. J. Ross, 1990: Prediction experiments of Hurricane Gloria (1985) using a multiply nested movable mesh model. *Mon. Wea. Rev.,* **118,** 2185–2198.

Liu, Y., D.-L. Zhang, and M. K. Yau, 1997: A multiscale numerical study of Hurricane Andrew (1992). Part I: Explicit simulation and verification. *Mon. Wea. Rev.,* **125,** 3073–3093.

——, ——, and ——, 1999: A multiscale numerical study of Hurricane Andrew (1992). Part II: Kinematics and inner-core structures. *Mon. Wea. Rev.,* in press.

Moss, M. S., and R. W. Jones, 1978: A numerical simulation of hurricane landfall. NOAA Tech. Memo. ERL NHEML-3, 15 pp. [Available from NOAA Library, 4301 Rickenbacker Cswy., Miami, FL 33149.]

Powell, M. D., 1982: The transition of the Hurricane Frederic boundary layer wind field from the open Gulf of Mexico to landfall. *Mon. Wea. Rev.,* **110,** 1912–1932.

——, and S. H. Houston, 1996: Hurricane Andrew's landfall in south Florida. Part II: Surface wind fields and potential real-time application. *Wea. Forecasting,* **11,** 329–349.

——, and ——, 1999: Comments on ''A multiscale numerical study of Hurricane Andrew (1992). Part I: Explicit simulation and verification.'' *Mon. Wea. Rev.,* **127,** 1706–1710.

——, ——, and T. A. Reinhold, 1996: Hurricane Andrew's landfall in South Florida. Part I: Standardizing measurements for documentation of the surface wind fields. *Wea. Forecasting,* **11,** 304–328.

Tao, W.-K., and J. Simpson, 1993: The Goddard cumulus ensemble model. Part I: Model description. *Terr. Atmos. Ocean. Sci.,* **4,** 35–72.

Tuleya, R. E., and Y. Kurihara, 1978: Numerical simulation of the landfall of tropical cyclones. *J. Atmos. Sci.,* **35,** 242–257.

——, M. A. Bender, and Y. Kurihara, 1984: A simulation study of the landfall of tropical cyclones using a movable nested-mesh model. *Mon. Wea. Rev.,* **112,** 124–136.

Wakimoto, R. M., and P. G. Black, 1994: Damage survey of Hurricane Andrew and its relationship to the eyewall. *Bull. Amer. Meteor. Soc.,* **75,** 189–200.

Zhang, D.-L., and R. A. Anthes, 1982: A high-resolution model of the planetary boundary layer—Sensitivity tests and comparison with SESAME-79 data. *J. Appl. Meteor.,* **21,** 1594–1609.